

## Article

# A Late Jurassic Epithermal Pb-Zn Deposit: Insights from Rb-Sr Dating of Quartz-Hosted Fluid Inclusions and Sphalerite Chemical Composition

Zheng Xia <sup>1,2</sup>, Zengxia Zhao <sup>1,2,\*</sup>, Xiang Zou <sup>1,2</sup> and Lei Liu <sup>1,2</sup>

<sup>1</sup> Guangxi Key Laboratory of Hidden Metallic Ore Deposits Exploration, Guilin University of Technology, Guilin 541004, China; xia\_zheng163@163.com (Z.X.); 15573412620@163.com (X.Z.); liulei@glut.edu.cn (L.L.)

<sup>2</sup> Collaborative Innovation Center for Exploration of Nonferrous Metal Deposits and Efficient Utilization of Resources in Guangxi, Guilin University of Technology, Guilin 541004, China

\* Correspondence: zhaozx@glut.edu.cn

**Abstract:** The Kangjiawan Pb-Zn deposit, situated within the Shuikoushan polymetallic ore field in Changning, Hunan Province, China, is a large-scale Pb-Zn deposit unearthed in 1976. Based on detailed geological field investigations, this study presents the results of the Rb-Sr isotopic dating, electron probe microanalyses (EPMAs), and LA-ICP-MS analyses of the Kangjiawan Pb-Zn deposit in order to determine the ore-forming age and the occurrence of trace elements in sphalerite and thereby constrain the genesis of the deposit. The Rb-Sr dating of quartz-hosted fluid inclusions yielded an Rb-Sr isochron age of  $150 \pm 4$  Ma, with an initial  $^{87}\text{Sr}/^{86}\text{Sr}$  ratio of  $0.71101 \pm 0.00008$  (MSWD = 1.1), suggesting that the Pb-Zn mineralization of the Kangjiawan deposit took place during the Late Jurassic, coeval with the magmatic activities within the ore field. EPMA and LA-ICP-MS analyses showed that Fe, Mn, and Cd were primarily incorporated into the sphalerite lattice through isomorphous substitution. Specifically, Fe and Mn substituted for Zn, whereas Cd replaced both Fe and Zn. Other elements such as Cu, Sb, and Sn occurred within the sphalerite lattice through mineral micro-inclusions or isomorphic substitution. EPMAs and LA-ICP-MS results showed that the FeS contents in sphalerite were less than 14.33%, with corresponding ore-forming temperatures below 259 °C. The LA-ICP-MS results showed that sphalerites from the Kangjiawan Pb-Zn deposit had relatively high Ga/In ratios ranging from 0.01 to 144, providing further support for medium-to-low-temperature mineralization. The trace element compositions of sphalerites from the Kangjiawan Pb-Zn deposit exhibit skarn-type characteristics, suggesting a potential association with contemporary magmatic activities within the Shuikoushan ore field. During the Late Jurassic, extensive granitic magmatic activities occurred in the study area. At the late stage of magma crystallization, hydrothermal fluid containing Pb and Zn precipitated at medium-to-low temperatures and generated the Kangjiawan Pb-Zn deposit.

**Keywords:** Rb-Sr dating; sphalerite elemental composition; ore-forming temperature; genesis of deposit; Kangjiawan Pb-Zn deposit



**Citation:** Xia, Z.; Zhao, Z.; Zou, X.; Liu, L. A Late Jurassic Epithermal Pb-Zn Deposit: Insights from Rb-Sr Dating of Quartz-Hosted Fluid Inclusions and Sphalerite Chemical Composition. *Minerals* **2024**, *14*, 485. <https://doi.org/10.3390/min14050485>

Academic Editors: Panagiotis Voudouris, Stylianos Tombros, Degao Zhai and Yucai Song

Received: 19 March 2024

Revised: 21 April 2024

Accepted: 30 April 2024

Published: 2 May 2024



**Copyright:** © 2024 by the authors. Licensee MDPI, Basel, Switzerland. This article is an open access article distributed under the terms and conditions of the Creative Commons Attribution (CC BY) license (<https://creativecommons.org/licenses/by/4.0/>).

## 1. Introduction

Southern Hunan is an important source of nonferrous metals, rare earth metals, and radioactive minerals in China. It is also an important part of the Nanling metallogenic belt, which is rich in W, Sn, Mo, Bi, Be, Pb, Zn, REE, Nb, Ta, and others. The Kangjiawan Pb-Zn deposit, located within the Shuikoushan polymetallic ore field in Changning, Hunan Province, is a large, concealed deposit discovered relatively recently with the highest annual output in the Shuikoushan ore field [1,2]. The ore bodies primarily occur in laminated and lenticular forms within a strongly silicified and fractured breccia zone, situated between the Permian Dangchong Formation marlstone and Qixia Formation limestone [3,4]. Therefore, some scholars believe that the deposit might be of a sedimentary genesis and controlled

via stratigraphy, lithology, petrography, and folding-fracture factors. However, the mineralization process and the genesis of the deposit are still under debate, in particular, the relationship between mineralization and magmatic activity [1,5], the source of ore-forming materials [6–8], and the properties and evolution of ore-forming fluids [1,6,9–12]. Several views on the genesis of the deposit have been proposed as follows: magma hydrothermal metasomatic filling [5,12–14]; polygenetic compound stratum [6,7]; and sedimentation–exhalation [9]. Recent studies on H-O and S isotopes from the area suggest that the Kangjiawan Pb-Zn deposit was a metasomatic deposit filling in silicified breccias [14]. At present, the deepest hole drilled in the deposit has reached 1500 m. However, no pluton related to mineralization has been found [15]. Hence, further investigation is necessary to elucidate the metallogenic process and origin of the Kangjiawan Pb-Zn deposit.

In this paper, we present a study of the geochronology and geochemistry of the Kangjiawan Pb-Zn deposit based on detailed geological field work, with new results from quartz Rb-Sr dating and data on sphalerite chemical compositions, in an attempt to constrain the deposit’s ore-forming age and mineralization process.

### 2. Ore Field Geological Setting

The Shuikoushan ore field is situated on the northwest margin of the Cathaysia Block, covering an area of ca. 240 km<sup>2</sup> (Figure 1). It is a large-scale polymetallic ore field renowned for its abundant reserves of metals such as Pb, Zn, Au, Ag, etc. The ore field encompasses multiple deposits, including the Kangjiawan Pb-Zn deposit, the Shuikoushan Pb-Zn deposit, the Longwangshan gold deposit, the Xianrenyan gold deposit, and the Shi’aoling Pb-Zn deposit (Figure 1b). In recent years, new discoveries of metal mineral resources, including Fe, Cu, and Mo, have been made in the ore field. It stands as one of China’s most crucial sources for the production of nonferrous metals and precious metals.

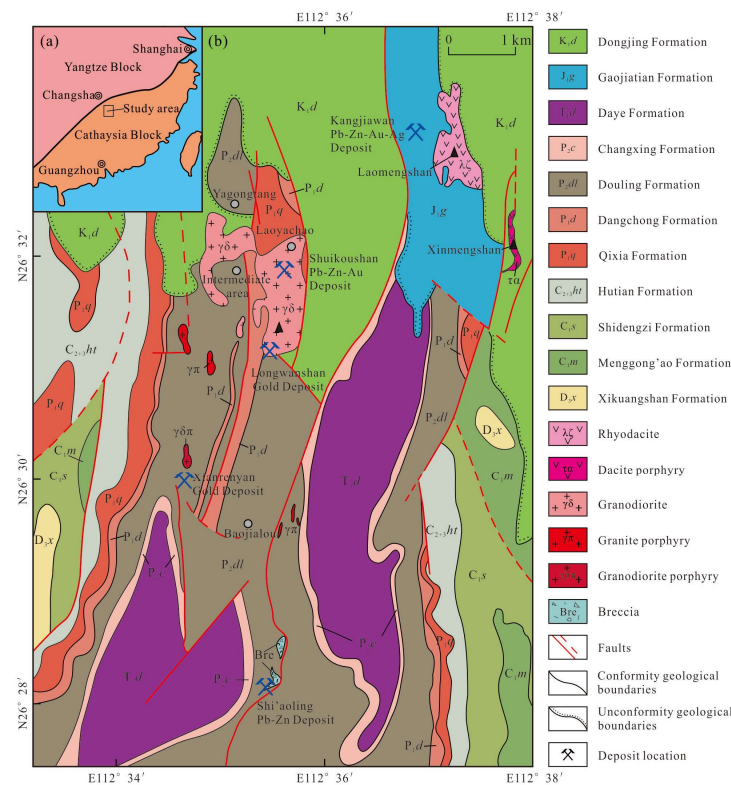


**Figure 1.** Tectonic setting (a) and geological map (b) of the Shuikoushan ore field (modified after Li and Peng [16]).

The Shuikoushan ore field primarily contains strata from the Paleozoic Devonian to the Cenozoic, with a total sedimentary thickness exceeding 3 km [16]. The strata below

the Upper Triassic are predominantly shallow marine carbonates interbedded with iron- and coal-bearing coastal plain sands and shales; meanwhile, the Upper Triassic to the Cretaceous strata are primarily composed of terrestrial clastic molasses. Among them, the Permian Qixia Formation comprises a series of thick-bedded limestones, exhibiting fracturing in its middle and upper sections due to the presence of flint and carbonaceous rocks. The lower section of the Permian Dangchong Formation is characterized by thin- to medium-bedded marlstones, whereas the upper section is comprised of Mn-bearing siliceous rocks, intermittently interrupted by thin layers of shale. These two formations are the main ore-bearing strata in the ore field.

Structures are actively developed within the Shuikoushan ore field, with fold hinges predominantly exhibiting a near-SN orientation, and fault structures primarily striking close to SN, followed by NE, NW, and EW (Figure 1b). These structures influence magmatic activity and mineralization processes within the ore field, closely associated with the widespread silicified breccias in the area.

Magmatic rocks are widely exposed in the Shuikoushan ore field, comprising a total of 72 identified plutons and occupying an area of ca. 4.8 km<sup>2</sup> (Figure 1b). These rocks consist of granodiorite, quartz diorite, rhyodacite, and dacite porphyry, followed by granodiorite porphyry, granite porphyry, and intermediate-acid lava rocks, with emplacement timing primarily attributed to the Late Jurassic [2,17–19]. They exhibit metaluminous to weak peraluminous characteristics, falling within the high-K calc-alkaline series with I-type affinities. It is proposed that the magmatic activity in the Shuikoushan ore field might originate from a mixture of the depleted mantle and the lower crust of South China and might be related to the extension in the lithosphere induced by the subduction of the Paleo-Pacific plate over 150~160 Ma [5,19,20].

### 3. Deposit Geology

The Kangjiawan Pb-Zn deposit is located in the northeastern part of the Shuikoushan ore field, approximately 3 km from the southwest Shuikoushan Pb-Zn deposit (Figure 1b) and serves as the ore field's primary mining site for Pb-Zn. The ore bodies are primarily situated within the interbedded silicified breccias, occurring between the marlstone of the Permian Dangchong Formation and the limestone of the Qixia Formation (Figure 2). The predominant geological structure of the ore bodies is stratabound, with secondary occurrences of lenticular and vein-like structures. To date, a cumulative total of 61 ore bodies have been delineated, among which seven are recognized as the principal deposits. The Kangjiawan Pb-Zn deposit is a large-scale Pb-Zn deposit characterized by metal reserves of about 220,000 tons of Pb, 240,000 tons of Zn, 750,000 tons of sulfur, 2 tons of Au, and 15 tons of Ag, with average ore grades of 3.92% for Pb, 4.50% for Zn, 2.68 g/t for Au, and 86.80 g/t for Ag.

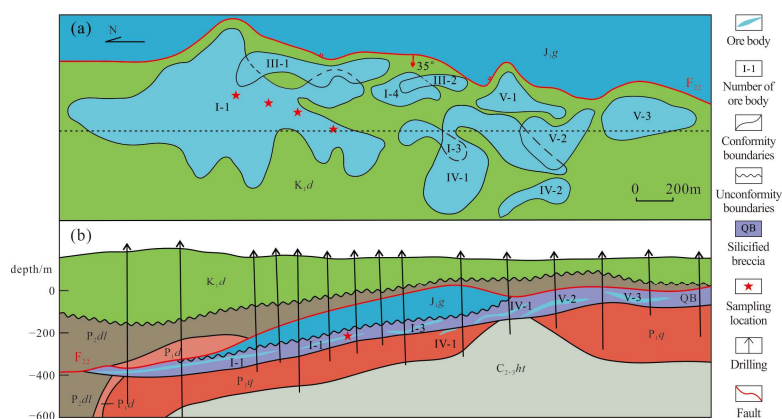


**Figure 2.** Geological profile of the Kangjiawan Pb-Zn deposit, (a) plan view, (b) elevation view. The dashed line in (a) shows the trace of the section in (b).

The ore minerals in the deposit predominantly include galena, sphalerite, and pyrite, with minor occurrences of chalcopyrite, arsenopyrite, and magnetite. Native gold and native silver are also sporadically encountered. Gangue minerals consist mainly of calcite, quartz, and chalcedony, followed by dolomite and trace amounts of chlorite (Figures 3 and 4).

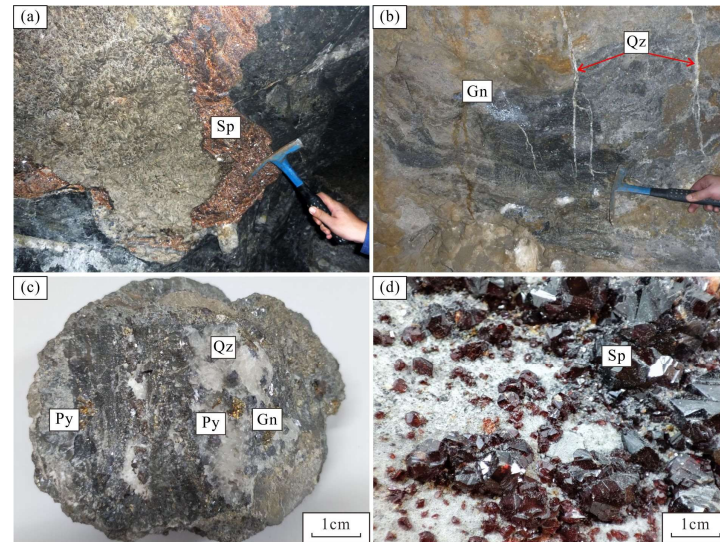


**Figure 3.** Underground ore photographs (a,b) and hand specimen images (c,d) for the Kangjiawan Pb-Zn deposit: (a) sphalerite vein of stage II; (b) quartz veins of stage III crosscut galena of stage II; (c) hand specimen of stage I; and (d) sphalerite of stage II. Sp—sphalerite; Gn—galena; Py—pyrite; Qz—quartz.

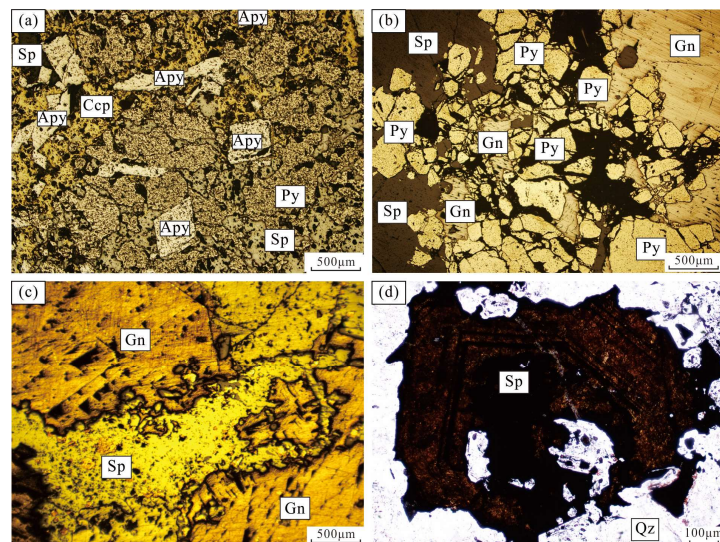


**Figure 4.** (a) Euhedral structure of arsenopyrite grains; (b) fractured structure of pyrite; (c) metasomatic texture: sphalerite replaces galena; (d) zoning structure of sphalerite. (All samples in this figure are from stage II; (a–c) represent photomicrographs under reflected light, while (d) depicts a transmitted light photomicrograph). Sp—sphalerite; Gn—galena; Py—pyrite; Apy—arsenopyrite; Ccp—chalcopyrite; Qz—quartz.

The ore exhibits various structures, including euhedral to subhedral grain structures (Figure 4a), fractured structures (Figure 4b), metasomatic structures (Figure 4c), zoning structures (Figure 4d), brecciated structures, colloform structures, skeleton structures, and granular structures. Structural formations include vein structures (Figure 3a), banded structures (Figure 3b), impregnation structures (Figure 3c), and massive structures

(Figure 3d), followed by flexural structures, angular fragment structures, and colloidal structures. The ore types primarily encompass galena–sphalerite–gold–pyrite–quartz ores, galena–sphalerite–gold–pyrite–calcite ores, galena–sphalerite–gold–pyrite–dolomite ores, and pyrite–quartz or pyrite–calcite ores.

Alterations in the surrounding rock are predominantly characterized by silicification, followed by carbonate alteration, minor fluoritization, sericite alteration, and chloritization, with localized occurrences of hornfels alteration and silicocarbonatite [21].

The mineralization of the Kangjiawan Pb–Zn deposit can be divided into three stages: (I) a pre-mineralization stage characterized by quartz–pyrite, (II) the main mineralization stage featuring quartz–pyrite–galena–sphalerite ores, and (III) the late-mineralization stage involving calcite–pyrite–galena–sphalerite ores (Figure 3) [22].

#### 4. Sampling and Analytical Methods

All samples were collected from Kangjiawan from underground stopes. Suitable samples were prepared as polished sections, which were subsequently subjected to mineralogical observations employing both reflected and transmitted light. Six samples from ore-bearing quartz veins were used for the Rb–Sr dating of fluid inclusions. Seven ore samples were designated for electron probe microanalysis (EPMA) on sphalerite, while five ore samples were allocated for the LA-ICP-MS spot analysis of trace elements in sphalerite. All the samples mentioned above belong to the main mineralization stage. The Rb–Sr analyses were carried out at the Isotopic Laboratory, Wuhan Geological Survey Center, China Geological Survey, while EPMA and LA-ICP-MS analyses were conducted at the Guangxi Key Laboratory of Hidden Metallic Ore Deposits Exploration, Guilin University of Technology, Guilin, China.

Six quartz samples of ore-bearing quartz veins were collected from the Kangjiawan Pb–Zn deposit. The samples were crushed into small specimens (less than 0.4 mm in diameter) and hand-picked carefully from each sample under a binocular microscope. The Rb–Sr analyses in this study were carried out using a MAT-261 mass spectrometer (Thermo Scientific, Waltham, MA, USA) following the methods of Li et al. [23]. During the analysis, repeat measurements on the standard NBS 987 sample yielded mean  $^{87}\text{Sr}/^{86}\text{Sr}$  ratios of  $0.71025 \pm 6$  ( $2\sigma$ ); on NBS 607, they yielded mean  $^{87}\text{Sr}/^{86}\text{Sr}$  ratios of  $1.20035 \pm 10$  ( $2\sigma$ ); and on GBW0411, they yielded mean  $^{87}\text{Sr}/^{86}\text{Sr}$  ratios of  $0.76006 \pm 15$  ( $2\sigma$ ) [23]. The total analytical blanks for Rb and Sr were 1–4 pg and 1–2 pg, respectively. The decay constant used for  $^{87}\text{Rb}$  was  $1.42 \times 10^{-11} \text{ a}^{-1}$ .

The EPMA analyses were performed with a JEOL JXA-8300 electron microprobe (JEOL Ltd., Tokyo, Japan). Prior to analysis, the specimens underwent uniform carbon coating with a coating thickness of 20 nm. The analytical parameters were as follows: a 15 kV accelerating voltage, a 20 nA beam current, and a 2  $\mu\text{m}$  spot size. Matrix correction was implemented through the ZAF correction program (Ver.1.14.0), resulting in a precision exceeding 1%. The elements measured included Zn, S, Fe, Mn, Cd, Pb, Cu, In, Co, As, Bi, Nb, Sn, Ti, Mo, Sb, Ga, and Ni.

The LA-ICP-MS analysis employed the GeoLas Pro HD laser ablation system (GeoLas Systems GmbH, Aschau im Chiemgau, Germany), featuring a laser beam spot diameter of 35  $\mu\text{m}$  and a laser ablation frequency of 10 Hz. The laser fluence was 3.5  $\text{J}/\text{cm}^2$ , with a repetition rate of 6 Hz. The ICP-MS utilized was the Agilent 7500 Series (Agilent Technologies, Santa Clara, CA, USA), which was calibrated using the NIST 610 standard glass (National Institute of Standards and Technology, Gaithersburg, MD, USA) to achieve a low oxide production rate. Each time-resolved analytical dataset comprised a 20 s blank signal and a 50 s sample signal. Helium carrier gas at a flow rate of 0.7 L/min was introduced into the cup, and the resulting aerosol was subsequently blended with Ar make-up gas at a rate of 0.89 L/min. The elements subjected to measurement included Ti, Mn, Fe, Co, Ni, Cu, Ga, Ge, Mo, Ag, Cd, In, Sn, Sb, Au, Tl, and Pb. The Zn content, as determined via EPMA, served as the internal standard, and outliers were excluded from the analysis.

### 5. Results

#### 5.1. Rb-Sr Dating of Fluid Inclusions in Quartz

The analytical Rb-Sr isotopic data of quartz-hosted fluid inclusions from the Kangjiawan Pb-Zn deposit are given in Table 1. Six samples exhibit <sup>87</sup>Rb/<sup>86</sup>Sr ratios ranging from 0.272 to 2.759. The isochron ages and initial <sup>87</sup>Sr/<sup>86</sup>Sr ratios were calculated using GeoKit software [24], with a 2% error for the <sup>87</sup>Rb/<sup>86</sup>Sr ratios and a 0.1% error for the <sup>87</sup>Sr/<sup>86</sup>Sr ratios (2σ). Six samples from the ore-bearing quartz veins yielded an Rb-Sr isochron age of 150 ± 4 Ma, with an initial <sup>87</sup>Sr/<sup>86</sup>Sr ratio of 0.71101 ± 0.00008 (MSWD = 1.1) (Figure 5).

**Table 1.** The analytical Rb-Sr isotopic data of quartz-hosted fluid inclusions from the Kangjiawan Pb-Zn deposit.

No.	Sample	Mineral	Rb/ppm	Sr/ppm	<sup>87</sup> Rb/ <sup>86</sup> Sr	<sup>87</sup> Sr/ <sup>86</sup> Sr	1σ
1	KJW020	Quartz	0.975	7.546	0.373	0.71159	0.00004
2	KJW032(2)	Quartz	0.222	0.232	2.759	0.71689	0.00003
3	KJW033	Quartz	0.227	0.455	1.438	0.71408	0.00005
4	KJW44-4	Quartz	0.722	3.252	0.640	0.71240	0.00002
5	KJW47	Quartz	0.327	1.846	0.510	0.71225	0.00001
6	KJW50	Quartz	1.009	10.710	0.272	0.71163	0.00007

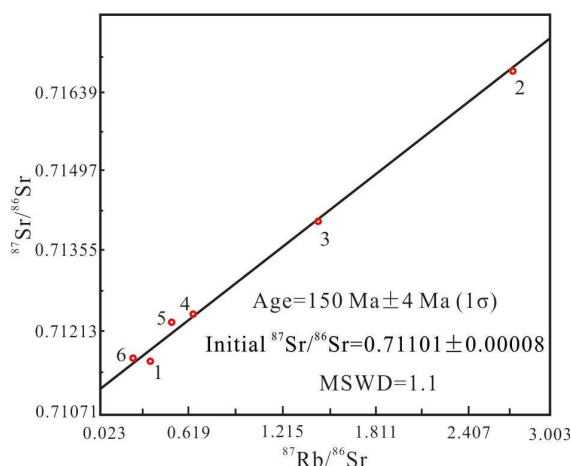


**Figure 5.** Rb-Sr isochron of fluid inclusions in quartz from ore bodies in the Kangjiawan Pb-Zn deposit. MSWD—Mean Standard Weighted Deviation. The numbers 1–6 represent the sample No. in Table 1.

#### 5.2. EPMA of Sphalerite

Seven sphalerites from the Kangjiawan Pb-Zn deposit were analyzed, and the results are listed in Table 2.

**Table 2.** EPMA of sphalerite from the Kangjiawan Pb-Zn deposit (wt.%).

Spot No.	As	Bi	Pb	Nb	Sn	Cu	Co	Ti	S	Mo	In	Sb	Mn	Cd	Ga	Zn	Ni	Fe	Total
K21-01-01	-	0.04	0.02	-	0.07	-	-	-	32.82	0.45	-	0.02	1.26	0.05	0.03	63.22	0.01	2.19	100.17
K21-01-02	0.02	-	-	-	-	0.01	-	-	33.18	0.52	0.01	-	1.74	0.06	0.05	60.93	0.02	3.81	100.35
K21-01-03	-	-	-	0.04	-	-	0.01	0.02	33.14	0.50	-	-	1.83	0.06	0.06	62.90	-	2.47	101.02
K21-01-04	0.04	-	0.02	0.04	-	-	0.01	-	33.40	0.51	0.01	-	0.79	0.07	0.03	63.35	-	1.54	99.81
K21-01-05	-	-	-	-	-	-	-	-	33.05	0.45	-	-	1.59	0.06	0.05	62.14	-	2.56	99.89
K21-01-06	0.01	-	0.09	0.03	0.02	0.02	-	-	33.13	0.51	0.01	-	1.38	0.05	0.05	61.50	-	2.89	99.70
K21-01-07	-	-	-	-	-	-	0.01	-	32.72	0.44	-	-	1.25	0.04	0.01	62.36	-	3.29	100.12
K21-01-08	-	-	-	-	0.03	-	0.03	-	32.68	0.49	-	0.01	1.03	0.06	0.05	62.02	-	2.73	99.14
K21-01-09	-	-	-	-	-	-	-	0.01	33.24	0.50	-	-	1.37	0.09	0.04	63.17	-	1.46	99.89
K21-01-10	-	-	-	0.03	-	0.35	0.02	-	33.00	0.50	-	-	1.33	0.06	0.06	61.75	-	2.50	99.60
K21-01-11	-	-	-	0.02	-	0.01	0.01	-	33.16	0.48	-	-	0.97	0.05	0.03	62.07	-	2.90	99.70

Table 2. Cont.

Spot No.	As	Bi	Pb	Nb	Sn	Cu	Co	Ti	S	Mo	In	Sb	Mn	Cd	Ga	Zn	Ni	Fe	Total
K21-01-12	-	-	0.07	0.02	0.03	-	-	0.04	32.97	0.47	-	-	1.97	0.06	0.07	62.28	0.01	1.90	99.89
K21-01-13	-	0.05	-	0.03	0.02	-	-	0.02	32.98	0.48	-	-	1.11	0.06	0.06	61.99	-	2.59	99.40
K21-01-14	0.01	-	-	-	0.02	-	0.01	-	32.72	0.44	-	-	1.27	0.07	0.09	61.91	0.01	2.76	99.30
K21-03-01	0.04	-	-	0.04	0.01	-	0.01	-	33.49	0.49	-	0.01	3.81	0.07	0.10	54.57	-	7.53	100.17
K21-03-02	-	-	-	-	-	-	0.03	0.03	32.98	0.50	-	-	1.92	0.06	0.04	60.82	-	3.65	100.02
K21-03-03	-	-	-	-	-	0.35	-	-	33.01	0.45	-	-	2.98	0.05	0.02	58.15	0.02	4.89	99.93
K21-03-04	-	0.03	-	0.01	-	-	-	0.03	33.42	0.49	-	-	3.02	0.04	0.06	57.88	0.02	6.30	101.31
K21-03-05	0.02	-	-	0.03	-	0.81	-	-	32.62	0.53	-	0.03	1.69	0.05	0.06	60.97	-	3.41	100.22
K21-03-06	-	-	0.10	0.08	-	0.02	0.02	-	33.24	0.42	-	-	3.44	0.07	0.05	57.28	0.01	6.15	100.87
K21-03-07	-	-	-	-	0.05	0.20	-	-	33.18	0.50	-	-	3.49	0.05	0.05	57.98	0.02	5.52	101.06
K21-03-08	0.01	0.01	-	-	-	-	-	0.02	33.28	0.44	-	-	2.28	0.06	0.02	59.79	-	4.71	100.62
K21-03-09	-	-	-	-	-	-	0.01	-	33.54	0.49	-	-	2.79	0.06	0.03	58.50	-	5.22	100.64
K21-03-10	-	-	-	-	-	-	-	-	32.83	0.49	-	-	1.64	0.06	-	60.19	-	4.41	99.62
K21-03-11	0.02	-	-	0.05	-	0.02	-	-	33.01	0.49	0.03	-	1.77	0.05	0.05	60.40	-	4.41	100.30
K21-03-12	-	-	-	0.02	-	1.96	-	0.01	33.53	0.56	-	-	3.40	0.06	0.08	57.61	-	4.74	101.95
K21-04-01	0.04	-	-	-	-	-	0.01	-	32.69	0.49	-	-	2.47	0.07	0.06	59.39	0.02	4.25	99.49
K21-04-02	-	-	-	-	0.02	0.02	0.01	-	33.35	0.45	-	-	2.49	0.07	0.04	58.90	-	4.71	100.07
K21-04-03	0.01	-	-	-	-	-	-	0.03	32.74	0.46	-	-	0.67	0.09	0.06	65.66	-	0.07	99.78
K21-04-04	-	-	-	0.04	-	-	-	-	32.75	0.46	-	-	0.79	0.09	0.02	65.30	-	0.15	99.60
K21-04-05	-	-	-	0.02	0.01	-	-	-	33.14	0.53	-	-	3.68	0.08	0.02	57.75	0.01	6.84	102.06
K21-04-06	-	-	-	0.03	-	0.02	-	-	32.75	0.51	-	-	0.82	0.09	0.07	65.09	0.01	0.40	99.78
K21-04-07	0.03	-	-	0.02	0.04	0.04	-	-	33.26	0.51	-	-	1.46	0.08	0.06	60.42	0.01	3.41	99.33
K21-04-08	-	-	-	0.03	0.02	-	-	-	33.09	0.56	-	-	3.06	0.09	0.06	57.91	0.02	6.08	100.92
K21-04-09	-	-	-	-	-	-	-	0.01	32.81	0.54	-	-	1.98	0.08	0.04	59.93	-	4.27	99.66
K21-04-10	-	0.04	-	0.04	0.03	-	0.01	-	32.07	0.45	-	-	2.08	0.09	0.09	61.56	0.01	2.40	98.86
K21-04-11	0.01	-	0.07	0.01	-	-	-	0.01	33.18	0.51	-	0.01	1.56	0.08	0.06	61.07	0.02	3.53	100.12
K21-04-12	-	-	0.03	0.11	-	-	-	-	32.95	0.48	-	-	1.75	0.07	0.04	60.97	-	3.52	99.92
K21-05-01	0.01	-	-	0.01	-	-	0.02	0.01	32.97	0.46	-	-	2.48	0.06	0.06	58.90	0.01	4.08	99.06
K21-05-02	0.02	-	-	-	0.04	-	-	-	33.12	0.47	-	-	3.45	0.08	0.05	56.95	-	6.92	101.09
K21-05-03	0.01	-	0.05	-	-	-	-	-	33.29	0.46	-	-	3.49	0.07	0.06	56.16	-	8.00	101.59
K21-05-04	0.01	-	-	-	-	-	0.03	0.02	33.25	0.47	-	-	3.67	0.08	0.09	56.02	-	7.47	101.09
K21-05-05	-	0.05	-	0.02	0.03	-	-	-	32.99	0.47	-	-	2.37	0.07	0.09	59.08	-	4.75	99.92
K21-05-06	-	0.05	-	0.03	-	-	-	-	32.86	0.53	-	-	2.32	0.07	0.04	59.79	-	3.43	99.12
K21-05-07	-	-	-	-	0.01	0.01	0.02	-	33.34	0.50	-	-	2.68	0.09	0.05	58.67	0.02	5.42	100.81
K21-05-08	-	-	-	-	0.05	0.06	0.02	-	33.10	0.42	-	-	2.85	0.07	0.02	58.31	-	5.89	100.79
K21-05-09	-	-	-	0.01	0.02	0.78	0.02	0.01	33.16	0.53	-	-	3.01	0.07	0.08	57.38	-	5.81	100.89
K21-05-10	-	0.04	0.05	-	0.03	-	0.02	-	32.59	0.47	-	-	1.49	0.08	0.04	64.01	0.01	0.15	98.96
K21-05-11	-	-	-	0.06	-	-	0.02	-	33.01	0.52	-	-	2.16	0.08	0.06	58.98	-	5.15	100.05
K21-06-01	-	-	-	-	-	0.01	-	0.01	32.46	0.48	-	0.01	0.73	0.12	0.03	65.58	0.01	0.03	99.46
K21-06-02	-	-	-	0.02	-	-	0.01	-	32.16	0.49	-	-	1.05	0.12	0.06	65.90	-	0.04	99.85
K21-06-03	-	-	-	-	-	0.01	-	-	32.75	0.44	0.01	-	0.68	0.13	0.04	65.82	0.01	0.04	99.93
K21-06-04	0.01	-	-	-	0.02	-	-	-	32.15	0.45	0.02	0.01	1.03	0.12	0.07	65.78	-	0.06	99.70
K21-06-05	0.01	-	-	0.06	-	0.04	0.01	-	32.40	0.50	-	-	0.42	0.10	0.03	66.13	0.01	0.06	99.75
K21-06-06	-	0.08	0.06	-	-	-	0.02	-	32.21	0.50	-	-	1.39	0.12	0.05	64.81	0.01	0.04	99.31
K21-06-07	-	-	-	0.04	0.01	-	-	0.01	32.68	0.54	-	-	0.45	0.13	0.01	65.94	-	0.03	99.83
K21-06-08	0.01	-	-	-	-	0.02	-	-	32.57	0.53	-	0.01	0.69	0.11	0.07	66.03	-	0.05	100.07
K21-06-09	-	-	-	-	-	-	0.03	0.04	32.06	0.50	-	-	1.39	0.11	0.06	65.80	-	0.05	100.03
K21-06-10	0.05	-	-	0.02	-	-	-	0.02	32.32	0.43	-	-	0.51	0.12	0.05	66.20	0.01	0.04	99.77
K21-08-01	-	-	0.05	0.03	0.01	-	-	-	32.47	0.50	-	-	0.56	0.11	0.08	65.70	-	0.05	99.54
K21-08-02	-	-	-	0.02	0.01	-	-	0.04	32.47	0.48	0.01	-	0.88	0.10	0.06	65.15	-	0.07	99.28
K21-08-03	-	-	-	-	-	-	0.01	-	32.28	0.47	-	-	0.98	0.18	0.06	65.17	0.01	0.09	99.24
K21-08-04	-	-	-	-	-	-	-	-	32.70	0.47	-	-	1.64	0.20	0.03	64.88	0.01	0.12	100.04
K21-08-05	-	-	-	0.06	-	-	-	-	32.54	0.56	0.01	-	1.45	0.17	0.07	65.37	-	0.07	100.29
K21-08-06	-	0.02	-	-	-	-	-	-	32.29	0.49	-	-	1.73	0.14	0.04	64.85	0.01	0.06	99.62
K21-08-07	0.01	0.04	-	-	-	-	0.01	0.02	32.59	0.48	-	-	0.89	0.19	0.08	65.33	-	0.03	99.65
K21-08-08	-	-	-	-	-	-	-	0.01	32.37	0.48	-	-	1.26	0.22	0.03	64.93	0.01	0.06	99.38
K21-08-09	0.06	0.01	-	0.02	-	-	-	0.02	32.23	0.53	-	-	0.72	0.15	0.03	65.98	-	0.03	99.79
K21-08-10	0.01	-	-	0.06	0.02	-	0.02	-	32.30	0.49	0.01	-	1.72	0.14	0.08	65.64	-	0.04	100.53
K21-09-01	0.05	-	-	0.01	-	-	-	-	32.74	0.50	-	-	0.99	0.06	0.02	62.65	0.01	5.03	102.07
K21-09-02	-	0.02	-	0.09	-	-	0.01	-	32.47	0.44	-	-	0.87	0.05	0.04	62.14	0.01	3.63	99.76
K21-09-03	-	0.01	0.02	0.03	-	0.21	-	-	32.26	0.46	-	-	1.85	0.06	0.03	60.09	0.01	3.85	98.86
K21-09-04	0.03	-	-	-	0.03	0.30	0.01	-	32.74	0.53	-	-	1.56	0.07	0.04	60.41	0.01	4.57	100.29
K21-09-05	-	-	-	-	-	-	-	-	32.45	0.48	-	-	2.67	0.07	0.01	61.42	-	3.85	100.94
K21-09-06	-	-	0.04	-	0.03	0.01	0.02	-	32.65	0.53	-	-	3.54	0.06	0.07	59.82	0.01	4.69	101.46
K21-09-07	-	-	0.04	-	0.04	-	-	0.01	32.64	0.50	-	-	2.18	0.06	0.06	59.83	-	4.79	100.15
K21-09-09	0.02	-	0.05	-	0.05	0.39	-	0.03	32.81	0.49	0.02	-	2.54	0.07	0.03	59.16	-	5.08	100.73
K21-09-10	0.01	-	-	0.05	0.02	-	-	-	32.56	0.49	-	-	1.96	0.06	0.04	60.25	0.02	4.30	99.76
K21-09-12	-	-	0.03	-	-	-	-	-	32.64	0.51	-	0.01	1.45	0.05	0.05	60.96	0.01	4.36	100.07

Note: “-” represents a result below the detection limit.

The content of Zn in sphalerite ranges from 54.57 to 66.20 wt.%, with an average of 61.67 wt.%; the S content ranges from 32.06 to 33.54 wt.%, averaging 32.82 wt.%; the Fe content ranges from 0.03 to 8.00 wt.%, with an average of 3.02 wt.%; the Mn content ranges from 0.42 to 3.81 wt.%, averaging 1.82 wt.%; the Cd content ranges from 0.04 to 0.22 wt.%, averaging 0.08 wt.%; and the Ga content ranges from 0.01 to 0.10 wt.% (one sample was below the detection limit), averaging 0.05 wt.%.

It is noteworthy that the dispersed elements Cd and Ga present in sphalerites from the Kangjiawan Pb-Zn deposit meet their respective industrial-grade specifications (Cd: 0.01~0.09%; Ga: 0.01~0.02%) [25]. Consequently, particular consideration should be given to the comprehensive utilization of Cd and Ga during the mining operations.

### 5.3. LA-ICP-MS Analyses of Sphalerite

Table 3 presents the results of the LA-ICP-MS spot analysis conducted on five sphalerite samples. Spots analyzed in samples K21-01, K21-04, and K21-09 are dark-colored sphalerites, whereas those in samples K21-06 and K21-08 are light-colored sphalerites. The presence of trace elements within sphalerite displayed significant variations: Fe ranged from 6.19 to 125,315 ppm (mean: 21,097 ppm), Cd ranged from 317 to 4791 ppm (mean: 1358 ppm), Mn ranged from 0.01 to 12,979 ppm (mean: 2791 ppm), Ga ranged from 0.01 to 31.3 ppm (mean: 5.96 ppm), Ge ranged from 0.01 to 2.35 ppm (mean: 0.22 ppm), In ranged from 0.08 to 21.5 ppm (mean: 1.73 ppm), Cu ranged from 0.03 to 6026 ppm (mean: 302 ppm), Ag ranged from 0.01 to 17.8 ppm (mean: 2.95 ppm), and Pb ranged from 0.18 to 45.1 ppm (mean: 4.99 ppm). Additionally, elements such as Sn, Sb, Co, Ni, and Ti exhibited varying concentrations, spanning in ppm from several to dozens. Notably, dark-colored sphalerites exhibit evidently higher Fe, Mn, Ga, and In contents than light-colored sphalerites (Table 3).

**Table 3.** LA-ICP-MS results of sphalerite from the Kangjiawan Pb-Zn deposit (ppm).

Spot No.	Ti	Mn	Fe	Co	Ni	Cu	Ga	Ge	Mo	Ag	Cd	In	Sn	Sb	Au	Tl	Pb
K21-01-01	8.59	8476	50,525	0.08	0.43	60.0	26.5	0.18	0.01	0.80	3113	5.72	21.9	0.97	0.01	0.68	7.84
K21-01-02	9.37	7728	59,325	0.07	0.04	11.6	7.13	0.12	0.04	0.28	2949	2.34	0.91	0.07	0.03	-	16.3
K21-01-04	11.8	11,031	67,119	0.15	-	3431	18.7	0.28	0.09	5.66	2721	10.3	46.1	1.88	0.04	0.02	2.44
K21-01-05	9.80	4194	77,394	0.19	2.46	1675	28.0	1.82	0.28	17.8	3157	14.6	14.1	56.6	0.21	0.25	23.3
K21-01-06	5.97	6951	74,330	0.05	0.55	536	2.64	-	0.43	7.95	2748	21.5	15.9	25.9	0.05	0.05	6.32
K21-04-01	8.70	887	6980	0.05	0.14	80.8	7.84	0.23	0.08	16.2	3337	0.45	26.0	37.2	0.03	0.03	18.5
K21-04-02	8.72	11,227	125,315	0.02	-	259	30.2	2.35	0.07	5.10	3750	0.70	148	8.71	0.16	0.08	21.5
K21-04-03	12.0	11,819	108,799	-	0.32	200	28.8	0.06	0.14	2.05	3805	0.62	110	0.28	0.05	-	45.1
K21-04-04	8.81	11,928	91,372	-	0.21	254	24.5	0.23	0.15	5.89	4028	1.35	179	8.54	0.04	0.07	10.6
K21-04-05	6.39	8044	82,851	0.11	2.45	203	24.5	0.30	0.03	3.34	4133	1.13	145	1.80	0.01	-	19.2
K21-04-06	6.20	12,979	100,922	0.09	0.13	226	31.3	0.41	0.10	5.88	4791	1.72	154	7.41	0.02	0.03	7.34
K21-04-07	10.2	5236	109,430	0.03	0.16	27.7	11.6	0.23	-	1.44	2881	0.08	7.40	0.11	0.01	-	12.8
K21-06-01	0.01	0.01	21.7	0.11	0.05	17.5	2.98	0.15	0.01	9.59	508	0.02	2.85	14.6	0.12	-	4.58
K21-06-02	0.01	0.02	6.19	0.21	0.04	0.52	0.55	0.01	-	0.02	576	-	0.02	-	-	-	0.50
K21-06-03	-	0.02	7.48	0.15	0.05	1.13	0.48	0.02	-	0.16	602	0.04	0.51	0.24	-	-	1.35
K21-06-04	-	0.01	14.4	0.15	0.05	34.2	5.38	0.50	0.06	17.3	531	-	0.06	34.2	0.10	-	8.18
K21-06-05	-	0.02	8.83	0.18	0.05	0.60	0.20	0.02	0.11	0.02	618	-	0.03	-	-	-	0.76
K21-06-06	0.02	0.02	6.97	0.20	0.04	0.03	0.01	0.01	-	0.01	675	-	0.05	-	-	-	0.73
K21-06-07	-	0.01	7.72	0.27	0.03	0.34	0.02	-	0.10	0.02	699	-	0.03	-	-	-	0.58
K21-06-08	0.01	0.02	7.63	0.26	0.04	0.60	0.04	0.02	0.13	0.02	739	-	0.05	0.01	-	-	0.94
K21-06-09	0.01	0.02	8.30	0.25	0.06	5.76	0.52	0.02	0.04	3.13	691	0.01	0.97	5.35	0.02	-	2.40
K21-06-10	-	0.02	8.00	0.20	0.03	1.50	0.42	0.04	0.06	0.29	581	0.01	0.26	0.49	-	-	0.64
K21-06-11	-	0.02	8.20	0.21	0.04	10.4	1.34	0.07	0.03	5.19	659	0.07	2.28	7.72	0.04	-	2.80
K21-06-12	0.01	0.01	7.63	0.23	0.03	0.28	0.05	0.03	0.03	0.03	599	0.08	0.17	0.02	-	-	0.44
K21-08-01	0.01	0.03	10.8	0.81	0.08	0.24	0.06	0.03	0.03	0.05	604	-	0.03	0.03	-	-	2.06
K21-08-02	0.01	0.02	9.18	0.33	0.02	1.17	0.06	0.02	0.04	0.93	2500	-	0.12	0.89	0.01	-	1.66
K21-08-03	0.01	0.05	7.39	0.32	0.01	1.72	0.02	0.01	0.15	0.02	946	2.42	0.07	0.01	-	-	0.25
K21-08-04	-	0.05	7.44	0.41	0.02	2.10	0.04	0.01	0.43	0.03	1000	0.67	0.11	0.04	-	-	0.32
K21-08-05	0.01	0.05	7.41	0.39	0.02	2.22	0.89	0.03	0.14	0.05	825	0.36	0.65	0.04	-	-	0.28
K21-08-06	-	0.04	7.20	0.33	0.02	2.05	0.07	0.01	0.13	0.03	769	0.87	1.11	-	-	-	0.27
K21-08-07	0.01	0.04	8.20	0.31	0.01	13.0	0.73	0.03	0.33	2.67	864	0.85	5.39	5.85	0.01	-	1.85
K21-08-08	-	0.05	10.2	0.34	0.02	0.47	0.02	-	0.06	0.06	1017	0.39	0.04	0.02	-	-	0.18
K21-08-09	0.01	0.07	12.4	0.32	0.06	12.3	0.45	0.04	0.54	3.52	902	0.02	3.98	6.97	0.02	-	1.78
K21-08-10	-	0.03	10.2	0.34	0.04	4.26	0.10	0.01	0.10	1.24	920	0.01	2.24	1.68	-	-	0.87
K21-08-11	-	0.03	9.1	0.35	0.01	4.65	0.15	0.01	0.04	0.54	810	0.01	3.09	1.21	-	-	0.43
K21-08-12	-	0.04	10.3	0.35	0.03	21.7	1.51	0.12	0.05	12.6	983	0.12	0.90	23.0	0.04	-	6.47
K21-09-01	-	1966	4045	-	0.01	11.5	2.60	0.20	0.01	1.30	351	0.29	0.87	1.60	-	0.01	1.44
K21-09-02	0.01	5295	3875	-	0.01	76.1	0.79	0.23	-	0.88	349	0.61	0.09	0.44	-	-	0.76
K21-09-03	0.01	1639	3601	-	-	3.03	1.52	0.25	-	0.60	307	0.10	0.35	0.40	-	-	0.79
K21-09-04	-	3260	5194	-	-	6.51	2.37	0.20	-	0.39	346	0.20	0.68	0.10	-	-	0.20
K21-09-05	0.01	3917	5865	0.01	0.01	15.5	2.71	0.20	0.01	0.49	395	0.37	3.53	0.37	-	-	0.69
K21-09-06	0.01	3473	10,788	-	0.01	1218	3.37	0.26	0.02	1.21	382	0.08	0.91	1.00	-	-	0.34
K21-09-07	0.01	3885	10,042	-	0.05	6026	3.45	0.21	0.01	2.21	332	0.27	0.88	0.47	-	-	1.01
K21-09-08	0.01	2307	1940	-	0.01	19.7	2.23	0.21	-	0.81	321	0.21	1.53	0.02	-	-	0.35
K21-09-09	0.01	1942	1976	-	0.01	5.66	2.58	0.13	-	0.61	312	0.20	0.40	0.04	-	-	0.39
K21-09-10	-	1912	3818	-	-	10.4	2.44	0.22	-	1.63	407	0.10	2.62	0.11	-	-	0.28
K21-09-11	-	2081	1841	-	0.01	3.49	1.89	0.16	0.01	0.64	317	0.12	0.56	0.40	-	-	0.92
K21-09-12	0.01	1781	5094	0.01	-	9.41	2.33	0.20	-	0.77	348	0.16	3.91	0.54	-	-	0.57

Note: “-” represents a result below the detection limit.

## 6. Discussion

### 6.1. Ore-Forming Age

Comprehensive geological dating studies conducted over the past decade have constrained the timing of magmatic activities in the Shuikoushan ore field to the Early Jurassic. For example, Zhen et al. [17] obtained an age of  $156 \pm 1.2$  Ma for the Xianrenyan granite porphyry via zircon LA-ICP-MS U-Pb dating; Zuo et al. [18] reported an age of  $156.7 \pm 1.6$  Ma for the emplacement of the Laomengshan rhyodacite, also determined via zircon LA-ICP-MS U-Pb dating; Yang et al. [19], using SIMS zircon U-Pb dating, proposed that the Shuikoushan granitoid was intruded at  $158.3 \pm 1.2$  Ma.

The precise dating of mineral deposits is crucial for constraining the mineralization process and the associated tectonic setting. Compared to the abundant magmatic timing data, there have been relatively few reports on the ore-forming age of the Shuikoushan ore field. Previous research has mostly speculated that the ore field's mineralization was contemporaneous with its magmatic activity, based on structural features, ore body attitudes, and relationships between ore bodies and magmatic rocks. However, due to the lack of precise isotopic dating analyses, these speculations have not garnered unanimous acceptance. The ore-forming age within the Shuikoushan ore field remained undetermined until 2015, when Huang et al. [20] conducted Re-Os isotopic dating on molybdenite from the Shuikoushan Pb-Zn deposit, obtaining an isochron age of  $157.8 \pm 1.4$  Ma. The ore-forming age of the Kangjiawan Pb-Zn deposit has not been reported thus far. Furthermore, the latest drilling exploration data from the deposit indicate that no pluton related to mineralization was discovered at a depth of 1500 m, which limits the assessment of its ore-forming mechanism and of its relationship with magmatic activities in the ore field.

Many studies have implied that fluid inclusion Rb-Sr dating is suitable for obtaining accurate ore-forming ages [26,27]. Although neither Rb nor Sr occurs in the quartz lattice, they could be trapped interstitially in crystal defects, such as in fluid inclusions found in quartz, as indicated in previous studies [28]. For example, Rb and Sr concentrations in quartz-hosted aqueous fluid inclusions from the Pingshui gold deposit, Zhejiang Province, China, are 0.60–14.5 ppm and 6.55–33.9 ppm, respectively [29]; Rb and Sr concentrations in fluid inclusions in quartz from the Xujiacun gold deposit, Heilongjiang Province, China, are 1.33–9.45 ppm and 11.1–75.3 ppm, respectively [30]. Fluid inclusions in quartz from the Kangjiawan deposit have Rb and Sr concentrations of 0.222–1.009 ppm and 0.232–10.710 ppm, respectively, and yielded an Rb-Sr isochron age of  $150 \pm 4$  Ma, implying that the Kangjiawan Pb-Zn deposit mineralized during the Late Jurassic, coeval with the magmatic activities within the Shuikoushan ore field.

### 6.2. Trace Element Occurrence in Sphalerite

Trace elements in geological bodies commonly exist in the following forms: independent minerals, isomorphic inclusions, non-isomorphic inclusions (including solid melt inclusions, mechanical inclusions, micro-particles, or elements existing in the interstices or other voids within mineral crystals in the form of ions, molecules, gases, or liquids), adsorptions, and inclusions associated with organic matter [31–33]. The inter-relationships among various trace elements in minerals can serve as indicators of their occurrence, where isomorphism corresponds to a negative correlation and non-isomorphism corresponds to a positive correlation [34,35].

During the crystallization of sphalerite,  $Zn^{2+}$  in the lattice is often replaced by other ions with similar properties, such as  $Fe^{2+}$ ,  $Mn^{2+}$ ,  $In^{3+}$ ,  $Cd^{2+}$ , etc. Among these,  $Fe^{2+}$  and  $Zn^{2+}$  share similar geochemical properties, with equal ionic radii and the same valence in tetrahedral coordination, making  $Fe^{2+}$  the primary ion for substituting  $Zn^{2+}$  in sphalerite.

In conditions characterized by elevated temperature and low oxygen fugacity, the iron in the fluid predominantly manifests as  $Fe^{2+}$ , facilitating a substantial substitution of  $Zn^{2+}$  in the sphalerite lattice by  $Fe^{2+}$ , consequently inducing the darkening of the sphalerite's color. As the temperature decreases and oxygen fugacity increases, iron gradually transforms from  $Fe^{2+}$  to  $Fe^{3+}$ , preventing its entry into the sphalerite lattice.  $Cd^{2+}$  then takes the place of the

previous  $\text{Fe}^{2+}$  in the lattice positions, causing the color of sphalerite to lighten. Therefore, in conditions marked by elevated temperature and low oxygen fugacity, sphalerite tends to exhibit a relatively greater enrichment of  $\text{Fe}^{2+}$ , whereas, in contrasting conditions, it demonstrates a relatively greater enrichment of  $\text{Cd}^{2+}$ , resulting in a negative correlation between Fe and Cd [34,35]. In other words, the presence of light-colored sphalerite indicates lower Fe content and relatively lower ore-forming temperatures [36].

In sphalerite from the Kangjiawan Pb-Zn deposit, both Fe and Mn exhibit a conspicuous negative correlation with Zn (Figure 6a,b), implying that Fe and Mn primarily incorporate into the sphalerite lattice through isomorphous substitution, displacing Zn. A broader negative correlation between Cd and Fe content indicates that Cd engages in isomorphous substitution within the sphalerite lattice, displacing Fe (Figure 6c). Notably, a distinct negative correlation between Cd and Zn is evident in sphalerites with higher Zn contents (i.e., the light-colored sphalerite) (Figure 6d), indicating the isomorphous substitution of Cd for Zn. Consequently, Cd in light-colored sphalerite replaces both Fe and Zn through isomorphous substitution.

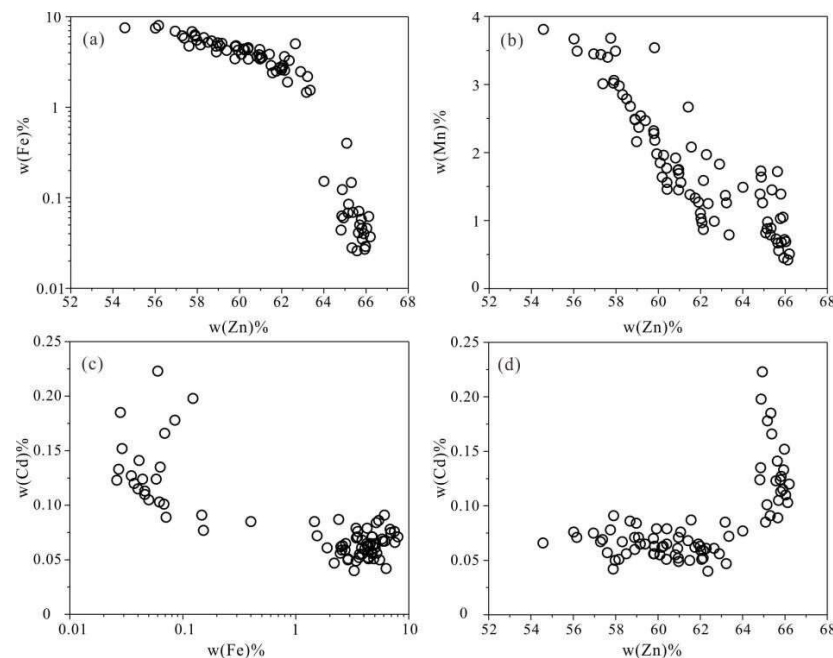


**Figure 6.** Diagrams of Fe vs. Zn (a), Mn vs. Zn (b), Cd vs. Fe (c), and Cd vs. Zn (d) for sphalerites from the Kangjiawan Pb-Zn deposit. All data presented in this figure are EPMA data.

Time-resolved profiles acquired through LA-ICP-MS analysis can effectively serve as indicators for elucidating the forms in which trace elements occur. A relatively flat appearance in the time-resolved spectrum of a specific element implies it has an isomorphic presence, whereas the presence of multiple peaks in the time-resolved spectrum for a given element signifies its occurrence in the form of mineral micro-inclusions [36–39]. In the LA-ICP-MS time-resolved profiles of sphalerites from the Kangjiawan Pb-Zn deposit (Figure 7), the time-resolved spectra for Fe, Mn, Cd, and In exhibit predominantly flat characteristics in the two representative samples, suggesting their prevalent isomorphic occurrence within the sphalerite matrix. Conversely, elements such as Cu, Sb, and Sn exhibit notable fluctuations in the curves of sample K21-01-06 (Figure 7a), while presenting smoother profiles in sample K21-01-01 (Figure 7b). In contrast, Pb exhibits an inverse pattern, displaying a smooth curve in sample K21-01-06 (Figure 7a) and pronounced fluctuations in sample K21-01-01 (Figure 7b). These observations suggest a coexisting state for these elements, indicating both the presence of mineral micro-inclusions and the potential for isomorphic substitution within the sphalerite lattice [40].

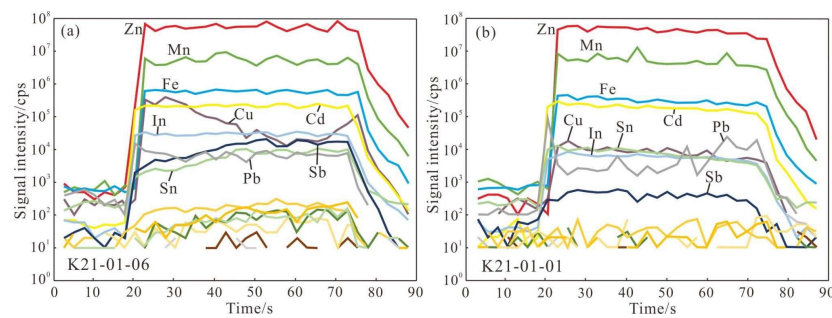


**Figure 7.** Representative LA-ICP-MS time-resolved profiles for sphalerites of sample K21-01-06 (a) and sample K21-01-01 (b) from the Kangjiawan Pb-Zn deposit.

### 6.3. Ore-Forming Temperature

The concentrations of trace elements in sphalerite exhibit a close correlation with the ore's formation temperature. Consequently, ore-forming temperatures can be ascertained by analyzing the trace element concentrations and their corresponding ratios in sphalerite [41–44]. For instance, sphalerite formed at elevated temperatures tends to exhibit greater enrichment in Fe, Mn, and In, while sphalerite formed under lower temperatures typically displays greater enrichment in Cd, Ga, Ge, and Zn. Therefore, the FeS content within sphalerite could serve as an indicative parameter for discerning ore-forming temperatures [45,46]. In the Kangjiawan Pb-Zn deposit, 79 EPMA data points and 48 LA-ICP-MS data points exhibited that the molar content of FeS in sphalerite ranged from below 0.01% to 14.33%. Notably, only 49 data points (consisting of 39 EPMA and 10 LA-ICP-MS data points) were plotted on the temperature evolution curve and obtained valid temperatures of 175 °C to 259 °C (Figure 8). Meanwhile, the remaining 78 data points failed to provide precise temperatures due to their significantly low FeS contents. It is evident that the formation temperatures of these low-iron sphalerites (i.e., the light-colored sphalerites) are significantly lower than high-iron ones (i.e., the dark-colored sphalerites) (Figure 8). Previous microthermometric analyses of fluid inclusions revealed that the transparent, light-colored sphalerites from the Kangjiawan Pb-Zn deposit precipitated at 120 °C to 140 °C [47]. These findings suggest that the sphalerites from the Kangjiawan Pb-Zn deposit formed under medium-to-low temperatures (lower than 259 °C).

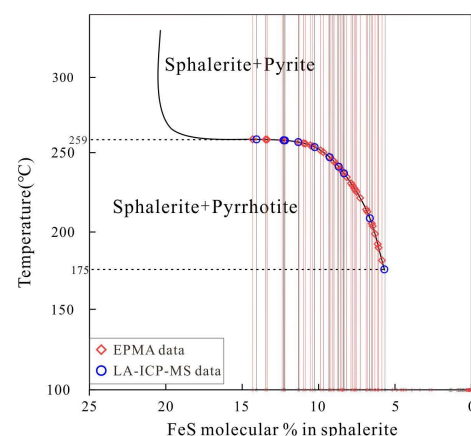


**Figure 8.** The diagram of temperature vs. molar content of FeS in sphalerite from the Kangjiawan Pb-Zn deposit (modified after Lu [45]). The red vertical line is the projection auxiliary line for EPMA data, while the black vertical line is the projection auxiliary line for LA-ICP-MS data.

Furthermore, the Ga/In ratio in sphalerite can serve as an additional criterion for assessing ore-forming temperatures. At low temperatures, the Ga/In ratio typically falls within the range of 1 to 100; at medium temperatures, it ranges from 0.01 to 5; and at high temperatures, the ratio is less than 0.01 [41,48]. The LA-ICP-MS results reveal that the Ga/In ratios in

sphalerite from the Kangjiawan Pb-Zn deposit range from 0.01 to 144, providing further support for classifying mineralization as occurring under medium-to-low temperatures.

#### 6.4. Genesis of the Deposit

The genesis of the Kangjiawan Pb-Zn deposit has been subject to debate for a long time, with several prevailing viewpoints currently put forward. These theories state that the genesis of the deposit is of the middle-temperature, hydrothermal contact, metasomatic type [1], the shallow-sourced, low-temperature, hydrothermal type [49,50], the paleokarst type [51], the silicification-reconstructed diatreme type [52], the normal sedimentary type [53], the stratabound type [7,54], or the skarn type [13]. Different Pb-Zn deposits of varying genetic origins exhibit distinct fluid properties and physicochemical conditions, resulting in notable differences in the trace element contents of the sphalerite [36,38]. Previous researchers have established discrimination diagrams for genetic types based on the compositional characteristics of sphalerite in Pb-Zn deposits of different types [36,38] (Figure 9). In the majority of these diagrams, data points from the Kangjiawan Pb-Zn deposit primarily fall within or in close proximity to the range of skarn-type deposits, distinctly differentiating them from Mississippi Valley-type (MVT) and Volcanogenic Massive Sulfide (VMS) deposits (Figure 9a–c). This indicates that this deposit exhibits skarn-type affinities, implying a potential link to magmatic processes. However, in certain diagrams, deviations from the range of skarn-type deposits are observed (Figure 9d), possibly attributable to contamination by strata material or external fluids [44,55].

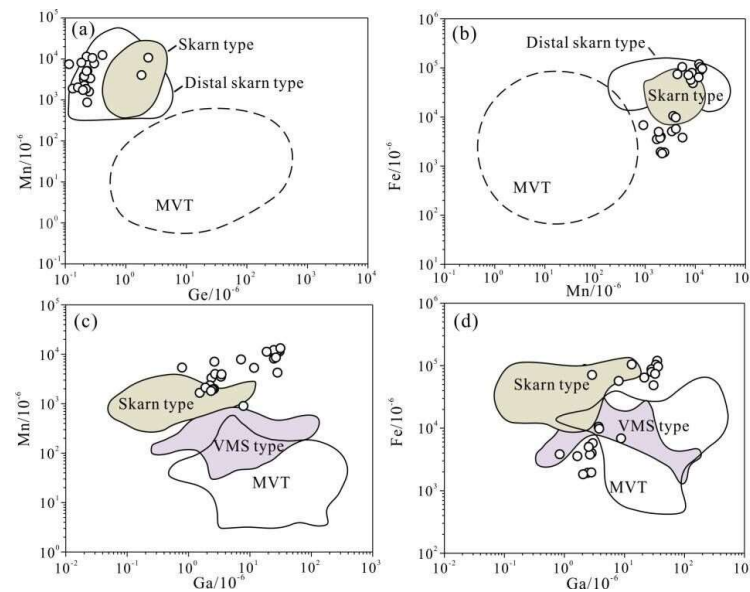


**Figure 9.** Diagrams of Mn vs. Ge (a), Fe vs. Mn (b), Mn vs. Ga (c), and Fe vs. Ga (d) for sphalerites from the Kangjiawan Pb-Zn deposit (modified after Cook et al. [36]; Ye et al. [38]). All data presented in this figure are LA-ICP-MS data.

The trace element composition of sphalerite can effectively serve as an indicator for discerning the genesis of Pb-Zn deposits. Previous studies have shown that deposits associated with magmatic or volcanic activities typically exhibit a relative enrichment of Fe, Mn, and In within sphalerite, while elements such as Ge and Tl tend to be depleted. Conversely, deposits related to basin brines show the opposite trend [36,38]. LA-ICP-MS analysis results indicate that the dark-colored sphalerites from the Kangjiawan Pb-Zn deposit exhibit significantly higher contents of Fe, Mn, and In (with average contents of 42,185 ppm, 5582 ppm, and 2.63 ppm, respectively), while the light-colored sphalerites yield lower contents of Fe, Mn, and In (with average contents of 9.29 ppm, 0.03 ppm, and 0.25 ppm, respectively). All the sphalerites have low contents of Ge (with an average content of 0.22 ppm) and Tl (with an average content of 0.14 ppm, most of which are

below the detection limit), suggesting a potential association with magmatic–hydrothermal activities during their mineralization process, especially the dark-colored sphalerites.

Previous studies indicated that Pb–Zn deposits associated with magmatic–hydrothermal processes exhibit specific characteristics in the trace element ratios of sphalerite, including  $Cd/Mn < 5$  and  $Cd/Fe < 0.1$  [48,56–58]. LA-ICP-MS analyses reveal that the dark-colored sphalerites from the Kangjiawan Pb–Zn deposit display low Cd/Mn ratios, ranging from 0.07 to 3.76, and low Cd/Fe ratios, ranging from 0.03 to 0.48. In contrast, the light-colored sphalerites demonstrate extraordinarily high Cd/Mn ratios, surpassing 12,000, and Cd/Fe ratios, exceeding 23. These data further support the inference that the mineralization of the Kangjiawan Pb–Zn deposit, particularly during the initial stages of main mineralization, was associated with magmatic–hydrothermal activities. Subsequently, as the mineralization temperature decreased, it may have been contaminated by other external substances.

In general, the comprehensive analyses of the aforementioned evidence suggest a mixed origin for the Kangjiawan Pb–Zn deposit. During the Late Jurassic, the deposit originated from a skarn-type environment, associated with contemporary magmatic activities within the Shuikoushan ore field, characterized by relatively high temperatures. Subsequently, the deposition of dark-colored sphalerites with higher Fe contents occurred under medium temperatures, while the precipitation of light-colored sphalerites with lower Fe contents took place under lower temperatures. The decrease in mineralization temperature may be attributed to the mixing of different fluids, such as meteoric water or strata water [2].

## 7. Conclusions

(1) The Rb–Sr dating of quartz-hosted fluid inclusions suggests that Pb–Zn mineralization of the Kangjiawan deposit took place during the Late Jurassic, with a Rb–Sr isochron age of  $150 \pm 4$  Ma.

(2) Fe, Mn, and Cd primarily incorporate into the sphalerite lattice through isomorphous substitution. Specifically, Fe and Mn substitute Zn, whereas Cd replaces both Fe and Zn. Other elements such as Cu, Sb, and Sn occur within the sphalerite lattice through mineral micro-inclusions or isomorphous substitution.

(3) The Kangjiawan Pb–Zn deposit formed under medium-to-low-temperature conditions ( $<259$  °C), as indicated by the relatively low FeS contents and high Ga/In ratios in sphalerite.

(4) The trace element compositions of sphalerites from the Kangjiawan Pb–Zn deposit exhibit skarn-type characteristics, suggesting a potential association with contemporary magmatic activities occurring within the Shuikoushan ore field.

**Author Contributions:** Conceptualization, Z.X. and Z.Z.; methodology, Z.X.; software, Z.X.; validation, Z.Z. and L.L.; formal analysis, Z.Z.; investigation, Z.X., X.Z. and Z.Z.; resources, Z.Z.; data curation, Z.X. and Z.Z.; writing—original draft preparation, Z.X.; writing—review and editing, Z.Z. and L.L.; visualization, Z.X.; supervision, Z.Z. and L.L.; project administration, Z.Z.; Data curation, X.Z.; funding acquisition, Z.Z. All authors have read and agreed to the published version of the manuscript.

**Funding:** This research was supported by the Natural Science Foundation of China (42263008), the Specific Research Project of Guangxi for Research Bases and Talents (Guike AD19110099), and the Guangxi Natural Science Foundation Program (2021GXNSFBA220063).

**Data Availability Statement:** The data is provided upon the request from the corresponding author due to the internal policy.

**Acknowledgments:** We sincerely thank Zhenglin Li and Yizhi Liu for their technical support in the sample analysis.

**Conflicts of Interest:** The authors declare no conflicts of interest.

## References

1. Yang, C.-Y. Discovery and genesis of the Kangjiawan lead-zinc deposit. *Geol. Prospect.* **1985**, *21*, 1–7. (In Chinese with English Abstract)
2. Zuo, C.-H.; Miao, B.-H.; Zhao, Z.-X.; Xu, Z.-W.; Lu, J.-J.; Lu, R.; Chen, J.-Q. A study on the isotopic geochemistry of Kangjiawan lead-zinc deposit, Changning county, Hunan province, China. *Acta Mineralogica Sin.* **2014**, *34*, 351–359. (In Chinese with English Abstract) [[CrossRef](#)]

3. Liu, S.-S. Geological characteristics of silicified Breccia in Shuikoushan lead zinc polymetallic ore field of Hunan and its association with mineralization. *Miner. Resour. Geol.* **2007**, *21*, 186–191. (In Chinese with English Abstract)
4. Ouyang, Z.-Q.; Shao, Y.-J.; Lian, C.-X.; Zang, Y. Geological characteristics and prospecting directions of Kangjiawan Pb-Zn-Au-Ag polymetallic deposit in Hunan. *Miner. Resour. Geol.* **2014**, *28*, 148–153. (In Chinese with English Abstract)
5. Zuo, C.-H. Study of the Kangjiawan Lead-Zinc Deposit Genesis and Relationship with Surrounding Magmatism in Changning City, Hunan Province. Doctor of Science. PhD Dissertation, Nanjin University, Nanjin, China, 2015. [[CrossRef](#)]
6. Liu, W. Nature, source and convection path of the ore-bearing fluid in Shuikoushan Pb-Zn-Au deposit. *Geotecton. Metallog.* **1994**, *18*, 209–218. (In Chinese with English Abstract) [[CrossRef](#)]
7. Bi, H. Discussion on mineralization of Kangjiawan lead-zinc-gold deposit in Hunan. *Gold Sci. Technol.* **1995**, *3*, 19–23. (In Chinese with English Abstract)
8. Liu, Q.-S. The metallogenic geologic conditions and metallogenesis of the Kangjiawan Pb-Zn deposit of the Shuikoushan polymetallic field in Hunan province. *Geol. Explor. Non-Ferr. Met.* **1996**, *5*, 340–346. (In Chinese with English Abstract)
9. Zhu, M.-X.; Lai, Y. The characteristics of mineral deposits related to geothermal activity and the possibility of existence of fossil geothermal zones in the Southeastern coastal area of China. *Reg. Geol. China* **1995**, *4*, 367–373. (In Chinese with English Abstract)
10. Liu, S.-S.; Tan, K.-X. *Dynamics of Ore-Forming in Open Systems—the Mechanism of Ore-Forming of the Shuikoushan Ore Field*; Seismological Press: Beijing, China, 1996.
11. Li, Y.-S.; Zhu, X.-Y.; Zhen, S.-M.; Gong, F.-Y.; Qi, F.-Y.; Gong, X.-D. Breccia characteristics of Kangjiawan lead-zinc-gold deposit in Hunan and its relationship with mineralization. *Miner. Depos.* **2010**, *29*, 963–964. (In Chinese with English Abstract) [[CrossRef](#)]
12. Zhang, B.-L. *Geochemical Study of Kangjiawan Lead-Zinc Deposit in Hunan Province*. Master's Thesis, Institute of Geochemistry Chinese Academy of Sciences, Guiyang, China, 2015. (In Chinese with English Abstract)
13. Quan, T.-J.; Zeng, W.-P. The prospecting history of Shuikoushan ore field and the prospecting direction of a new round of old mines. *Land Resour. Her.* **2006**, *3*, 70–74. (In Chinese with English Abstract)
14. Li, Y.-S.; Zhang, B.-L.; Gong, F.-Y.; Du, Z.-Z.; Zhen, S.-M. Genesis of the giant Kangjiawan lead-zinc ore deposit in Hunan Province: Evidences from fluid inclusion, H-O and S isotope. *Acta Petrol. Sin.* **2021**, *37*, 1847–1866. (In Chinese with English Abstract) [[CrossRef](#)]
15. Li, Y.-S.; Zhen, S.-M.; Gong, F.-Y.; Gong, X.-D.; Jia, D.-L.; Du, Z.-Z. The determination and significance of metallogenic geological body of Kangjiawan Pb-Zn-Au-Ag deposit in Hunan Province. *Acta Mineral. Sin.* **2011**, *S1*, 964–965. (In Chinese with English Abstract) [[CrossRef](#)]
16. Li, N.-Q.; Peng, C. *Shuikoushan Pb-Zn-Au-Ag deposit, Hunan Province*; Seismological Press: Beijing, China, 1996.
17. Zhen, S.-M.; Zhu, X.-Y.; Li, Y.-S.; Du, Z.-Z.; Gong, F.-Y.; Gong, X.-D.; Qi, F.-Y.; Jia, D.-L.; Wang, L.-L. Zircon U-Pb geochronology and Hf isotopic compositions of the monzonite, related to the Xianrenyan gold deposit in Hunan Province and its geological significances. *J. Jilin Univ. (Earth Sci. Ed.)* **2012**, *42*, 1740–1756. (In Chinese with English Abstract) [[CrossRef](#)]
18. Zuo, C.-H.; Lu, R.; Zhao, Z.-X.; Xu, Z.-W.; Lu, J.-J.; Wang, R.-C.; Chen, J.-Q. Characterization of element geochemistry, LA-ICP-MS zircon U-Pb age, and Hf isotope of granodiorite in the Shuikoushan deposit, Changning, Hunan province. *Geol. Rev.* **2014**, *60*, 811–823. (In Chinese with English Abstract) [[CrossRef](#)]
19. Yang, J.-H.; Peng, J.-T.; Zheng, Y.-F.; Hu, R.-Z.; Bi, X.-W.; Zhao, J.-H.; Huang, J.-C.; Zhang, B.-L. Petrogenesis of the Mesozoic Shuikoushan peraluminous I-type granodioritic intrusion in Hunan Province, South China: Middle-lower crustal reworking in an extensional tectonic setting. *J. Asian Earth Sci.* **2016**, *123*, 224–242. [[CrossRef](#)]
20. Huang, J.-C.; Peng, J.-T.; Yang, J.-H.; Zhang, B.-L.; Xu, C.-X. Precise zircon U-Pb and molybdenite Re-Os dating of the Shuikoushan granodiorite-related Pb-Zn mineralization, southern Hunan, South China. *Ore Geol. Rev.* **2015**, *71*, 305–317. [[CrossRef](#)]
21. Zhao, Z.-X.; Xu, Z.-W.; Zuo, C.-H.; Lu, J.-J.; Lu, R. Fluid Inclusion and stable isotope studies on Kangjiawan Pb-Zn-Au-Ag deposit, Hunan Province, South China. *Acta Geol. Sin. (Engl. Ed.)* **2014**, *88*, 1216–1217. [[CrossRef](#)]
22. Shen, H.-J.; Zhang, Y.; Zuo, C.-H.; Shao, Y.-J.; Zhao, L.-J.; Lei, J.-Z.; Shi, G.-W.; Han, R.-Y.; Zheng, X.-Y. Ore-forming process revealed by sphalerite texture and geochemistry: A case study at the Kangjiawan Pb-Zn deposit in Qin-Hang Metallogenic Belt, South China. *Ore Geol. Rev.* **2022**, *150*, 105153. [[CrossRef](#)]
23. Li, Q.-L.; Chen, F.-K.; Yang, J.-H.; Fan, H.-R. Single grain pyrite Rb-Sr dating of the Linglong gold deposit, eastern China. *Ore Geol. Rev.* **2008**, *34*, 263–270. [[CrossRef](#)]
24. Lu, Y.-F. GeoKit—A geochemical toolkit for Microsoft Excel. *Geochimica* **2004**, *33*, 459–464. (In Chinese with English Abstract)
25. Zhang, T.-D.; Liu, Z.-F.; Di, H.-F.; Zhang, J.-K.; Cheng, K.; Shao, Y.-J. Geochemical characteristics of sphalerite from the Baoshan deposit in southern Hunan and its implications for Cu-Pb-Zn-Ag polymetallic ore-forming mechanism. *Miner. Explor.* **2021**, *12*, 1716–1726.
26. Nakai, S.i.; Halliday, A.N.; Kesler, S.E.; Jones, H.D. Rb-Sr dating of sphalerites from Tennessee and the genesis of Mississippi Valley type ore deposits. *Nature* **1990**, *346*, 354–357. [[CrossRef](#)]
27. Shepherd, T.; Darbyshire, D. Fluid inclusion Rb-Sr isochrons for dating mineral deposits. *Nature* **1981**, *290*, 578–579. [[CrossRef](#)]
28. Pettke, T.; Diamond, L.W. Rb-Sr dating of sphalerite based on fluid inclusion-host mineral isochrons; a clarification of why it works. *Econ. Geol.* **1996**, *91*, 951–956. [[CrossRef](#)]
29. Ni, P.; Wang, G.-G.; Chen, H.; Xu, Y.-F.; Guan, S.-J.; Pan, J.-Y. An Early Paleozoic orogenic gold belt along the Jiang-Shao Fault, South China: Evidence from fluid inclusions and Rb-Sr dating of quartz in the Huangshan and Pingshui deposits. *J. Asian Earth Sci.* **2015**, *103*, 87–102. [[CrossRef](#)]
30. Tian, B.-Q.; Wang, S.-P.; Qi, Z.-Y. Rb-Sr Isochron age of fluid inclusions in the quartz of xujiaacun gold deposit, Heilongjiang Province. *Geol. Resour.* **2020**, *29*, 113–119. (In Chinese with English Abstract)

31. Dai, T.-G.; Liu, H.-Y. *Trace Element Geochemistry and Its Application*; Zhongnan University Press: Changsha, China, 1992.
32. Zhao, Z.-H.; Zhou, L.-D. REE geochemistry of some alkali-rich intrusive rocks in China. *Sci. China Ser. D* **1997**, *40*, 145–158. (In Chinese with English Abstract) [[CrossRef](#)]
33. Huang, F.; Wang, D.-H.; Li, C.; Wang, C.-H.; Liu, X.-X.; He, H.-H. Application of ICP-MS in the determination of trace elements in molybdenite. *Miner. Depos.* **2014**, *33*, 1167–1168. (In Chinese with English Abstract) [[CrossRef](#)]
34. Liu, T.-G.; Ye, L.; Zhou, J.-X.; Wang, X.-L. Cd primarily isomorphously replaces Fe but not Zn in sphalerite. *Acta Mineral. Sin.* **2010**, *30*, 179–184. (In Chinese with English Abstract) [[CrossRef](#)]
35. Shao, P.; Shi, D.-F.; Zi, F. Study on selective replacement characteristics of Fe and Zn by Cd in Sphalerite. *J. Hunan Univ. Sci. Technol. (Nat. Sci. Ed.)* **2020**, *35*, 27–32. (In Chinese with English Abstract) [[CrossRef](#)]
36. Cook, N.J.; Ciobanu, C.L.; Pring, A.; Skinner, W.; Shimizu, M.; Danyushevsky, L.; Saini-Eidukat, B.; Melcher, F. Trace and minor elements in sphalerite: A LA-ICP-MS study. *Geochim. Cosmochim. Acta* **2009**, *73*, 4761–4791. [[CrossRef](#)]
37. Benedetto, R.D.; Bernardini, G.P.; Costagliola, P.; Plant, D.; Vaughan, D.J. Compositional zoning in sphalerite crystals. *Am. Mineral.* **2005**, *90*, 1384–1392. [[CrossRef](#)]
38. Ye, L.; Cook, N.J.; Ciobanu, C.L.; Liu, Y.-P.; Zhang, Q.; Liu, T.-G.; Gao, W.; Yang, Y.-L.; Danyushevskiy, L. Trace and minor elements in sphalerite from base metal deposits in South China: A LA-ICPMS study. *Ore Geol. Rev.* **2011**, *39*, 188–217. [[CrossRef](#)]
39. Ye, L.; Li, Z.; Hu, Y.; Huang, Z.; Zhou, J.; Fan, H.; Danyushevskiy, L. Trace elements in sulfide from the Tianbaoshan Pb-Zn deposit, Sichuan Province, China: A LA-ICP-MS study. *Acta Petrol. Sin.* **2016**, *32*, 3377–3393. (In Chinese with English Abstract)
40. Leng, C.-B.; Qi, Y.-Q. Genesis of the Lengshuikeng Ag-Pb-Zn Orefield in Jiangxi: Constraint from In-situ LA-ICPMS Analyses of Minor and Trace Elements in Sphalerite and Galena. *Acta Geol. Sin.* **2017**, *91*, 2256–2272.
41. Liu, Y.-J.; Cao, M.-L.; Li, Z.-L.; Wang, H.-N.; Chu, T.-Q. *Geochemistry of Element*; Geological Press: Beijing, China, 1984.
42. Wang, J.-C.; Yu, D.-L. The distribution characteristics and geological significance of Cadmium and Iron in sphalerite—A case study of the Pb-Zn deposit in Xitieshan, Qinghai. *Miner. Explor.* **2011**, *2*, 720–728. (In Chinese with English Abstract)
43. Ye, L.; Gao, W.; Yang, Y.-L.; Liu, T.-G.; Peng, S.-S. Trace elements in sphalerite in Laochang Pb-Zn polymetallic deposit, Lancang, Yunnan province. *Acta Petrol. Sin.* **2012**, *28*, 1362–1372. (In Chinese with English Abstract)
44. Frenzel, M.; Hirsch, T.; Gutzmer, J. Gallium, germanium, indium, and other trace and minor elements in sphalerite as a function of deposit type—A meta-analysis. *Ore Geol. Rev.* **2016**, *76*, 52–78. [[CrossRef](#)]
45. Lu, H.-Z. Sphalerite geological thermometer and pressure gauge. *Geol. Geochem. Features* **1975**, *2*, 6–9. (In Chinese with English Abstract)
46. Yu, Q.-H.; Li, R.-Q.; Feng, Z.-T. *Typomorphic Characteristics of Sphalerite in Lead-Zinc Deposits in Nanling Area. Collection of Papers on Mineralogy of the First National Symposium on Mineralogy*; Geological Press: Beijing, China, 1987; pp. 80–85.
47. Zuo, C.-H.; Zhao, Z.-X.; Xia, Z.; Liu, L.; Zuo, Z.; Wang, T.-Y. Ore-forming mechanism of the Kangjiawan Pb-Zn Deposit, southern Hunan Province: Evidence from fluid inclusions. *J. Guilin Univ. Technol.* **2023**; *web premiere*. (In Chinese with English Abstract)
48. Kang, K.; Du, Z.-Z.; Yu, X.-F.; Li, Y.-S.; Lv, X.; Sun, H.-R.; Du, Y.-L. LA-ICP-MS trace element analysis of sphalerite in Huaniushan Pb-Zn deposit in Gansu Province and its geological significance. *J. Jilin Univ. (Earth Sci. Ed.)* **2020**, *50*, 1418–1432. (In Chinese with English Abstract)
49. Hu, Z.-J.; Wu, Y.-F. Localization modes of ore deposits in the Shuikoushan ore field and the assessment for potential prospecting area. *Geol. Prospect.* **2005**, *41*, 17–21. (In Chinese with English Abstract)
50. Zhang, Q.-H. The geological characteristics of the Shuikoushan lead-zinc ore field in Hunan and the prospecting thought clues. *Geol. Explor. Non-Ferr. Met.* **1999**, *8*, 141–146. (In Chinese with English Abstract)
51. Shi, J.-K.; Wang, Q.-H. The discovery and prospecting significance of diwa(geodepression)-type paleo-karst U-Au deposit in Shuikoushan mining area, Hunan Province. *Carsologica Sin.* **1986**, *51*, 115–125. (In Chinese with English Abstract)
52. Liu, L.-J.; Wang, Q.-H.; Shi, J.-K. Palaeo-karst sedimentary formation of diwa(geodepression) stage in Southern China. *Acta Sedimentol. Sinica* **1991**, *9*, 44–52. (In Chinese with English Abstract) [[CrossRef](#)]
53. Xu, D.-R.; Liu, J.; Chen, G.-H. Petrochemical characters of silicified breccia in the Kangjiawan poly-metallic deposit, Changning, Hunan. *Chin. J. Geol.* **2002**, *37*, 356–364. (In Chinese with English Abstract)
54. Zhu, M.-X.; Lai, Y.; Zhu, W.-J.; Shen, M.-Z. Ancient geothermal activity and its geology implications in Shuikoushan ore area, Hunan Province China. *Sci. Geol. Sin.* **1997**, *6*, 195–202.
55. Lockington, J.A.; Cook, N.J.; Ciobanu, C.L. Trace and minor elements in sphalerite from metamorphosed sulphide deposits. *Mineral. Petrol.* **2014**, *108*, 873–890. [[CrossRef](#)]
56. Han, Z.-X. The typomorphic characteristic of the sphalerite in the Qinling devoniansystem lead-zinc metallogenic belt. *J. Xian Coll. Geol.* **1994**, *16*, 12–17. (In Chinese with English Abstract) [[CrossRef](#)]
57. Cao, H.-W.; Zhang, S.-T.; Zhen, G.; Liu, R.-P.; Tian, H.-H.; Zhang, X.-H.; Li, J.-J. Geochemical characteristics of trace element of sphalerite in the Zhongyuku (Pb)-Zn deposit of the Luanchuan, Southwest of China. *Miner. Pet.* **2014**, *34*, 50–59. (In Chinese with English Abstract)
58. Tian, H.-H.; Zhang, S.-T.; Cao, H.-W.; Han, J.-W.; Lv, P.-R.; Zhang, Y.-H. Geochemical characteristics of trace elements of sphalerite in the Chitudian Pb-Zn deposit, West Henan Province. *Bull. Mineral. Petrol. Geochem.* **2015**, *34*, 334–342. (In Chinese with English Abstract)

**Disclaimer/Publisher’s Note:** The statements, opinions and data contained in all publications are solely those of the individual author(s) and contributor(s) and not of MDPI and/or the editor(s). MDPI and/or the editor(s) disclaim responsibility for any injury to people or property resulting from any ideas, methods, instructions or products referred to in the content.